Optical characterization of $Zn_{0.95-x}Be_xMn_{0.05}Se$ mixed crystals

D. O. Dumcenco,[1,*] C. T. Huang,[1] Y. S. Huang,[1,†] F. Firszt,[2] S. Łęgowski,[2] H. Męczyńska,[2] A. Marasek,[2] and K. K. Tiong[3]

[1]*Department of Electronic Engineering, National Taiwan University of Science and Technology, Taipei 106, Taiwan*

[2]*Institute of Physics, N. Copernicus University, Grudziądzka 5/7, 87-100 Toruń, Poland*

[3]*Department of Electrical Engineering, National Taiwan Ocean University, Keelung 202, Taiwan*

(Received 25 February 2009; revised manuscript received 22 April 2009; published 26 June 2009)

A systematic study of a series of $Zn_{0.95-x}Be_xMn_{0.05}Se$ mixed crystals with different Be content ($0.05 \leq X \leq 0.20$) grown by the modified high-pressure Bridgman method were carried out by room-temperature surface photovoltage spectroscopy (SPS), temperature-dependent photoluminescence (PL), and contactless electroreflectance (CER). A typical PL spectrum at low temperature consists of free exciton line, an edge emission due to recombination of shallow donor-acceptor pairs, and the Mn^{2+}-related intraionic emission. The near band-edge transition energies determined by analyzing the CER and SPS spectra showed a blueshift with the increase in Be content. The peak positions of band-edge exciton features in the PL spectra shifted slightly toward lower energies as compared to the corresponding transition energies obtained from CER and SPS data. The observed increases in the CER-PL shift with the increasing of Be content are explained by the increasing compositional disorder causing the smearing of the band-edge energies. The excitonic line broadening for the samples with larger Be/Zn ratio are attributed in part to the alloy-scattering effects and also to the poorer crystalline quality of the samples with higher content of Be. In addition, the parameters that describe the temperature dependence of the transition energies and broadening parameters of the band-edge excitonic transitions were evaluated and discussed.

DOI: 10.1103/PhysRevB.79.235209 PACS number(s): 75.50.Pp, 78.20.−e, 78.55.Et, 78.68.+m

I. INTRODUCTION

In recent years ZnSe-based diluted magnetic semiconductors obtained by alloying of zinc selenide with beryllium and manganese chalcogenides received great attention for their potential application in magnetoelectronics.[1] Be-chalcogenide semiconductor alloys have been recently proposed for improving the performance of ZnSe-based blue-green lasers.[2,3] According to theoretical calculation,[4] it is known that due to its large amount of covalent bonding and high cohesive energy, the beryllium-based bonding can be used to enhance the crystal elastic rigidity in II-VI alloys. It is expected that the incorporation of beryllium will lead to bond strengthening within the II-VI lattice,[5] and also will increase the energy of stacking-fault formation, thus reducing defect propagation that has been seriously limiting the lifetimes of ZnSe-based devices. The interest in manganese containing II-VI mixed crystals results from the electrical inactivity of Mn in II-VI semiconductors and its relative high solubility to form solid solutions with many II-VI binary compounds.[6,7] For this reason II-VI mixed crystals with Mn as a constituent offer an unique possibility of controlling magnetic properties and electrical conductivity independently in contrast to III-V compounds with Mn.[8,9] The novel and peculiar magnetic and magneto-optical properties of Mn-containing II-VI solid solutions arise from the interaction between charge carriers and the magnetic Mn^{2+} ion occupying the cation site in the crystal lattice.[10]

The quaternary $Zn_{1-x-y}Be_xMn_ySe$ mixed crystals are particularly attractive for their possible application in spintronics as a spin filter layers and memory technology. A partial substitution of Zn by Be offers a possibility to control the structure, lattice constant, and band parameters of the material, which is of great importance for application in multilayer optoelectronics technology. In particular, adding Be causes almost linear dependence of the value of energy gap and lattice constant on Be content and may stabilize the crystal structure.[11] Although the admixture of Mn only causes small change in the band-gap energy for Mn content less than about 20%, it influences the magnetic properties of the mixed crystals.[12] Hence, the variation in Be and Mn content allows obtaining $Zn_{1-x-y}Be_xMn_ySe$ semiconductor, which is an interesting material for spintronics with different energy gap and lattice constant matched to different substrates. To date, there are very limited published data concerning systematic investigation of II-VI quaternary diluted magnetic semiconductor thin layers[13] and bulk crystals.[14–16]

In this work, we reported the optical investigation of $Zn_{0.95-x}Be_xMn_{0.05}Se$ mixed crystals grown by the modified high-pressure Bridgman method from the melt with Be content from 0.05 to 0.20 using surface photovoltage spectroscopy (SPS) technique at room temperature, temperature-dependent photoluminescence (PL), and contactless electroreflectance (CER) in the temperature range of 10–300 K. The transition energies and broadening parameters of the band-edge excitonic features are determined by analyzing the PL and CER spectra. The effects of variation in Be content on properties of this quaternary $Zn_{0.95-x}Be_xMn_{0.05}Se$ series are presented. The parameters that describe the temperature dependence of the band-edge excitonic transitions were evaluated and discussed.

II. EXPERIMENTAL

The $Zn_{0.95-x}Be_xMn_{0.05}Se$ mixed crystals with $x=0.05$, 0.10, 0.15, and 0.20 denoted samples A, B, C, and D, respec-

tively, were grown from the melt by the high-pressure Bridgman method as described in Refs. 17 and 18. The crystals were cut into 1–1.5-mm-thick plates and mechanically polished. To remove mechanical defects on the surface, the samples were mechanically polished using successively finer abrasives with the final polishing process using 0.05 μm aluminum-oxide (Al_2O_3) powder. For optical measurements, samples were additionally etched in the mixture of $K_2Cr_2O_7:H_2SO_4:H_2O$ at the 3:2:1 proportion.[19]

In SPS measurement, the contact potential difference between the sample and a reference grid electrode was measured in a capacitive manner as a function of the photon energy of the probe beam by holding the grid fixed and chopping the probe beam with frequency 200 Hz.[20] It is known that, under low level of optical excitation, the surface photovoltage is proportional to the absorption coefficient.[21] Therefore, by monitoring the potential change when monochromatic light impinges on surface of the sample, it was possible to obtain relevant information on the energetic distribution of the joint density of states. The incident light intensity of a 150 W xenon arc lamp filtered by a Photon Technology Inc. 0.25 m monochromator was maintained at a constant level of 10^{-5} W/cm^2.

PL spectra were excited using the 325 nm line (~50 mW) of a He-Cd laser. The luminescence signals were analyzed by using a Jobin-Yvon "TRIAX 550" spectrometer equipped with a "SIMPHONY" charge-coupled-device camera. In CER measurements,[22] an ac modulating voltage (~1 kV at 200 Hz) was applied between the front wire grid electrode and the second electrode consisting of a metal plate. The probe beam entered through the front wire grid. The radiation from a 150 W xenon arc lamp filtered by a Photon Technology Inc. 0.25 m monochromator provided the monochromatic excitation light. The reflected light was detected by an UV-enhanced silicon photodiode. The dc output of this photodiode was maintained constant by a servomechanism of a variable neutral density filter. A dual-phase lock-in amplifier was used to measure the detected signals. The entire data-acquisition procedure was performed under computer control. Multiple scans over a given photon-energy range were programmed until a desired signal-to-noise level has been attained. A close-cycle cryogenic refrigerator equipped with a digital thermometer controller was used to control the measurement temperature between 10 and 300 K with a temperature stability of 0.5 K or better.

III. RESULTS AND DISCUSSION

A proper surface treatment of the sample must be performed to eliminate the damaged layer formed on the surface caused by mechanical polishing. The SPS technique could be utilized to check the condition of the surface layer.[23] Figures 1(a)–1(d) show, respectively, the evolution of the SPS spectra for $Zn_{0.95}Be_xMn_{0.05}Se$ mixed-crystal samples A, B, C, and D at room temperature. As shown in Fig. 1 the typical SPS spectrum has a steplike shape, which is characteristic of the excitonic transitions around the fundamental band edge. In order to determine the values of the transition energies, we numerically calculated the first derivative of the surface photovoltage signal (DSPS) with respect to photon energy $(\Delta V_{SPS}/\Delta E)$ and then divided this quantity by the value of the photovoltage itself V_{SPS}. The ratio $(\Delta V_{SPS}/\Delta E)/V_{SPS}$ is proportional to $(\Delta\alpha/\Delta E)/\alpha$,[24] where α is the absorption coefficient. The obtained curves are displayed by the dotted lines in Fig. 1. The full curves are least-squares fits to the first derivative of a Lorentzian line shape function of the form[25,26]

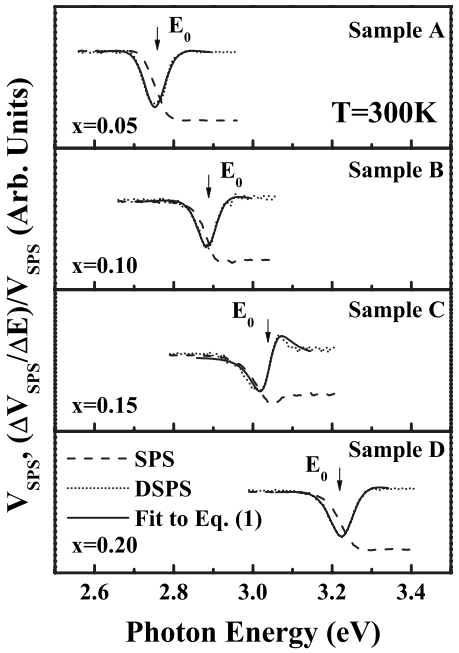

FIG. 1. Room temperature experimental SPS results as well as $(\Delta V_{SPS}/\Delta E)/V_{SPS}$ for $Zn_{0.95-x}Be_xMn_{0.05}Se$ with different Be content. The arrows show the position of the band-edge excitonic features obtained from DSPS by least-squares fits to Eq. (1) (solid line). The obtained values of the transition energies are indicated by the arrows.

$$\frac{\Delta R}{R} = \mathrm{Re}\sum_{j=1} A_j e^{i\Phi_j}(E - E_j + i\Gamma_j)^{-n}, \qquad (1)$$

where A_j and Φ_j are the amplitude and phase of the line shape, E_j and Γ_j are the energy and broadening parameter of the transitions, and the value of n depends on the origin of the transitions. The value of $n=2$ has been determined to be appropriate for excitonic transitions. As shown in Fig. 1, the near-band-edge excitonic transition E_0 indicated by an arrow exhibits blueshifted character with increasing of Be content. The excitonic transition energies obtained from SPS are listed in Table I.

Figures 2(a)–2(d) present the temperature evolutions of PL spectra for A, B, C, and D mixed-crystal samples, respectively. When $T=10$ K, the PL spectra consisted of a sharp peak corresponding to the highest energy in emission spectrum followed by a broader "edge-emission" band due to radiative recombination of shallow donor-acceptor pairs (DAP). Below 2.5 eV, at least two main features were observed for $Zn_{0.90}Be_{0.05}Mn_{0.05}Se$ and $Zn_{0.85}Be_{0.10}Mn_{0.05}Se$ samples, positioned at energies 2.0 and 2.35 eV. For

TABLE I. Values of the excitonic transition energies obtained from SPS, CER measurements, and peak positions of PL spectra for $Zn_{0.95-x}Be_xMn_{0.05}Se$ mixed crystals at room temperature. The parameters for ZB-$Zn_{0.75}Be_{0.05}Mn_{0.20}Se$, ZB-$Zn_{0.81}Be_{0.04}Mg_{0.15}Se$, ZB-$Zn_{0.96}Be_{0.04}Se$, and ZB-$Zn_{0.93}Mg_{0.07}Se$ are included for comparison.

Samples	E_{SPS} (eV)	E_{PL} (eV)	E_{CER} (eV)	E_{CER}-E_{PL} (meV)
$Zn_{0.90}Be_{0.05}Mn_{0.05}Se$ [a]	2.752	2.745	2.751	6
$Zn_{0.85}Be_{0.10}Mn_{0.05}Se$ [a]	2.887	2.880	2.888	8
$Zn_{0.80}Be_{0.15}Mn_{0.05}Se$ [a]	3.037	3.027	3.039	12
$Zn_{0.75}Be_{0.20}Mn_{0.05}Se$ [a]	3.229	3.217	3.232	15
ZB-$Zn_{0.75}Be_{0.05}Mn_{0.20}Se$ [b]		2.736	2.752	16
ZB-$Zn_{0.81}Be_{0.04}Mg_{0.15}Se$ [c]		2.873	2.886	13
ZB-$Zn_{0.96}Be_{0.04}Se$ [d]		2.784	2.790	6
ZB-$Zn_{0.93}Mg_{0.07}Se$ [d]		2.756	2.765	9

[a]Present work (SPS, CER, and PL).
[b]Reference 12 (CER and PL).
[c]Reference 39 (CER and PR).
[d]Reference 41 (CER).

$Zn_{0.95-x}Be_xMn_{0.05}Se$ samples with $x=0.15$ and 0.20 only the band with maximum at 2.0 eV was observed. This emission denoted as Mn^{2+} is the characteristic luminescence associated with Mn ions in II-VI compounds and is due to Mn^{2+} intraionic emission.[27] The photoluminescence-excitation (PLE) spectra with the emission detected at 2.0 eV (maximum of the yellow Mn emission) exhibited structure very well resolved at low temperatures. This transition was interpreted as related to the internal transitions in Mn ion. The lower the Mn content in the crystal, the better resolved the structure is. The energies of these particular components in PLE spectra were very close to energies of maxima in absorption spectrum of ZnS:Mn cubic single crystals observed by McClure[28] and Ryskin *et al.*[29] and could be interpreted as associated with transitions from the ground $^6A_1(^6S)$ state of Mn to the following different excited states: $^4T_1(^4G)$, $^4T_2(^4G)$, $(^4A_1, ^4E)(^4G)$, $^4T_1(^4P)$ or $^4T_2(^4D)$.[30] At low temperatures the luminescence spectra were similar when excited separately with each of the above mentioned energies and this confirmed the origin of this yellow emission as being due to Mn^{2+} intracenter transition.

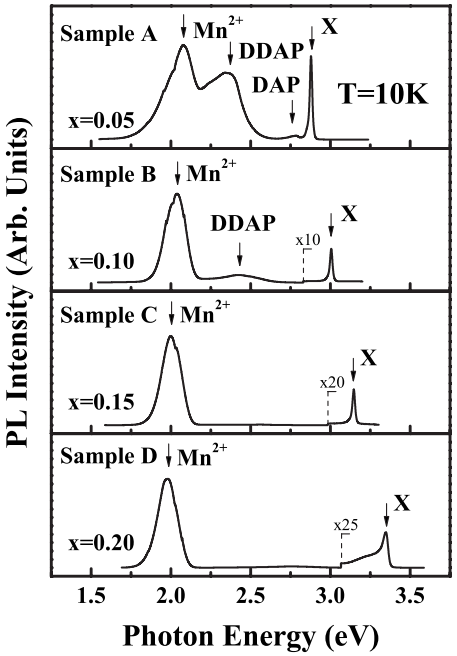

FIG. 2. The PL spectra of $Zn_{0.95-x}Be_xMn_{0.05}Se$ with different Be content measured at 10 K. The band-edge excitonic line, donor-acceptor pair emission, and Mn^{2+}-related intraionic emission bands are indicated by arrows.

From the PL spectra presented in Fig. 2 it is clearly seen that in the investigated series of $Zn_{0.95-x}Be_xMn_{0.05}Se$ crystals the energy gap increased, while the maximum of the yellow Mn-related emission decreased with the increasing of Be content. Applying the crystal-field theory it has been shown[31] that the energetic position of Mn-related PL is influenced by the bond length in the crystal. With increasing of beryllium content in $Zn_{0.95-x}Be_xMn_{0.05}Se$ crystals, the lattice constant decreases, causing increasing the value of the crystal field seen by Mn ion. This effect in turn modifies the energetic position of the first excited state $^4T_1(^4G)$ reducing the transition energy to the ground state $^6A_1(^6S)$.

The luminescence band positioned at 2.35 eV was related to deep D-A pairs transition where the acceptor responsible for this transition was a complex containing the cation vacancy as it was shown for $Zn_{1-x}Be_xSe$ and $Zn_{1-x}Mg_xSe$ by positron-annihilation experiment.[32,33] The values of energy position/full width at half maximum (FWHM) of the first peak X at 10 K were determined to be 2.878 ± 0.002 eV/17.2 ± 1.0 meV, 3.005 ± 0.002 eV/18.3 ± 1.0 meV, 3.152 ± 0.002 eV/19.6 ± 1.0 meV, and 3.347 ± 0.002 eV/22.2 ± 2.0 meV for samples A, B, C, and D, respectively. The peak position in $Zn_{0.95-x}Be_xMn_{0.05}Se$ samples series was found to be sensitive to the Be content, exhibiting a blueshift character for x value increasing from 0.05 to 0.20. The Be content dependence of the band-edge excitonic transition energies could be fitted by the expression (Ref. 34), $E_X(x)=E_X(0)+bx+cx^2$, where x is the concentration of Be, $E_X(0)$ is the appropriate energy in $Zn_{0.95}Mn_{0.05}Se$, and b and c are, respectively, the linear and nonlinear (bowing) parameters. This relation is customarily used to express the composition-dependent gap energy for the direct band gaps in mixed III-V semiconducting compounds. The obtained values for the fitting parameters were $E_X(0)=2.796$ eV, $b=1.3$ eV, and $c=7.2$ eV.

The values of FWHM were much larger than that of ZnSe,[35] indicating the difficulty of growing uniform ZnBeMnSe quaternary crystals and the influence of compositional disorder. The excitonic line broadening for the samples with larger Be/Zn ratio could be attributed in part to the alloy-scattering effects and also to the poorer crystalline quality of the samples with higher content of Be. The intensity of deep DAP emission diminished rapidly with increasing of Be content.

Figure 3 shows the temperature evolution of the near-band-edge PL spectra for samples A, B, C, and D, respectively. The low-temperature spectrum of sample A [Fig. 3(a)] consisted of a free exciton line, as confirmed by CER mea-

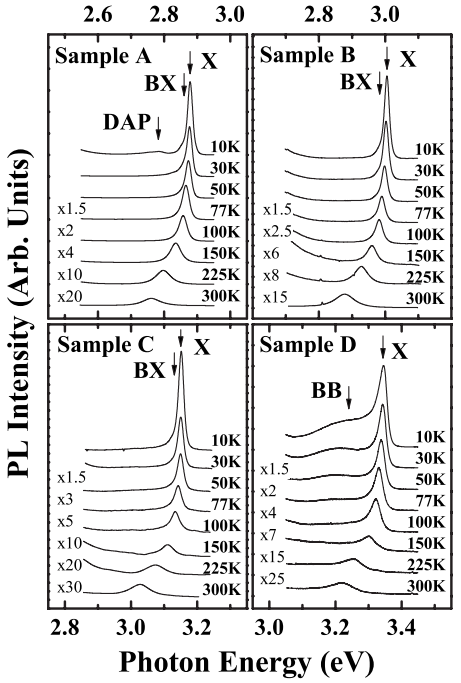

FIG. 3. The near-band-edge PL spectra of $Zn_{0.95-x}Be_xMn_{0.05}Se$ crystals at several temperatures between 10 and 300 K. The free exciton *X* and bound exciton *BX* lines, and shallow donor-acceptor pairs emission bands are indicated by arrows.

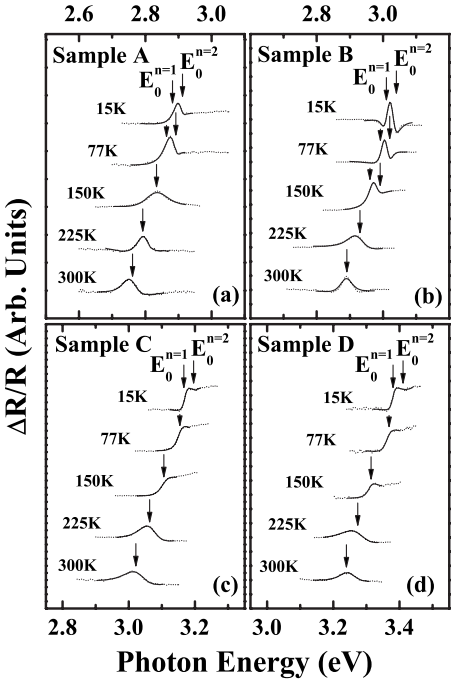

FIG. 4. Experimental CER spectra (dotted curves) of $Zn_{0.95-x}Be_xMn_{0.05}Se$ mixed-crystal samples at several temperatures between 15 and 300 K. The full lines are least-squares fits to Eq. (1). The obtained values of the transition energies are indicated by the arrows.

surement, and the so-called edge emission at 2.78 eV. The rather weak shoulderlike peak at 2.86 eV labeled as BX was assigned to the radiative recombination of exciton bound to some shallow defect center. With increasing of Be content [Figs. 3(b)–3(d)] the edge emission band at low temperature almost disappeared while BX feature could still be resolved. At the highest Be content ($x=0.20$), additional defect-related broad-band feature appeared near 3.25 eV. As shown in Fig. 3 the excitonic peak *X* shifted monotonically toward lower energy and broadened with temperature increasing in the range from 10 to 300 K. The values of excitonic peak energies at room temperature are listed in Table I.

The dotted curves in Figs. 4(a)–4(d) represent, respectively, the experimental CER spectra in the vicinity of the fundamental transitions for samples A, B, C, and D at temperatures 15, 77, 150, 225, and 300 K. These data were fitted to Eq. (1) and the results of such fitting were shown by the solid lines (see Fig. 4). For the first derivative functional form, $n=2$ is appropriate for the excitonic transitions. For M_0-type three-dimensional critical-point interband transitions, $n=0.5$ is appropriate.[25] At low temperature our experimental data had a better fit with $n=0.5$. We emphasize, however, that the transition energies extracted from such fits are relatively insensitive to the line-shape function. The anomaly of the fitting results might be related to the peculiar steplike shape around E_0 feature of the CER spectra. This kind of line shape is not common for CER experiment. This might be related to excitons bounded to local compositional fluctuations which were always present in Be/Mn-containing quaternary compounds. This argument was supported by the reduction in the steplike shape (Fig. 4) at higher temperatures where the excitons may not be bounded anymore. One should note here that this steplike line shape is not observed in some other II-VI wide band-gap materials such as ZnO.[36] This was probably due to better compositional uniformity of binary compounds than quaternary solid solutions.

The CER spectra at 15 K, see Fig. 4, consisted of two distinct features $E_0^{n=1}$ and $E_0^{n=2}$ indicated by vertical arrows. The energies $E_0^{n=1}$ and $E_0^{n=2}$ corresponded to the ground state and the first excited state of the band-edge excitonic transitions. The transition energies of $E_0^{n=1}/E_0^{n=2}$ at 15 K were determined to be $2.886\pm0.003/2.904\pm0.003$ eV, $3.015\pm0.003/3.035\pm0.005$ eV, $3.167\pm0.003/3.188\pm0.005$ eV, and $3.361\pm0.003/3.385\pm0.005$ eV for samples A, B, C, and D, respectively. Using the hydrogenic model, the binding energies of the band-edge exciton were determined to be 24 ± 6, 27 ± 6, 28 ± 6, and 32 ± 6 meV, for crystals A, B, C, and D, respectively. The binding-energy values were comparable with those obtained for $Zn_{1-x-y}Be_xMg_ySe$ mixed crystals.[37] As the temperature increases, the CER spectral features shifted toward lower energies (redshift) and broaden. The line broadening were mainly due to the increase in electron (exciton)-phonon interaction effects. The two features were not clearly resolved at temperatures higher than 150 K for $Zn_{0.95-x}Be_xMn_{0.05}Se$ crystals with low Be content and at temperatures higher than 77 K for crystals with Be content 0.15 and 0.20. We therefore fitted the spectra with only one feature, denoted as E_0, at higher temperatures. The fitted values of the transition energies for samples A, B, C, and D at 300 K agree quite well with SPS results (Table I).

The temperature variation in the experimental values of energies corresponding to excitonic transitions *X* with repre-

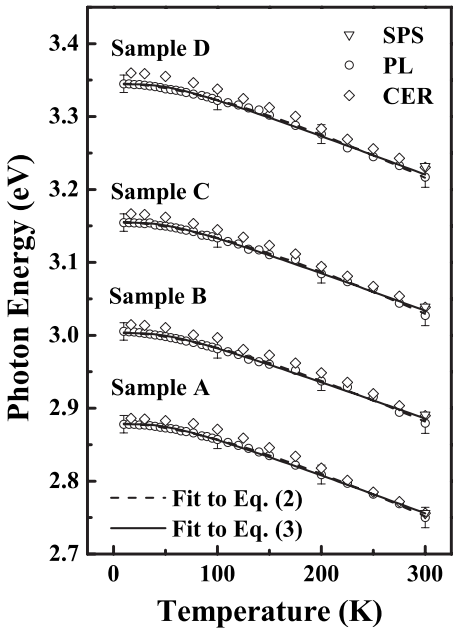

FIG. 5. Temperature variations in the experimental PL and CER values for excitonic transitions with representative error bars for $Zn_{0.95-x}Be_xMn_{0.05}Se$ depicted as open circles and open diamonds, respectively. Open triangles are the excitonic transitions obtained from DSPS at room temperature. The dotted lines are least-squares fits to Eq. (2) and the full curves are least-squares fits to Eq. (3).

sentative error bars obtained from PL spectra for the four investigated $Zn_{0.95-x}Be_xMn_{0.05}Se$ mixed crystals are depicted in Fig. 5 as open circles. For comparison purposes, the temperature dependence of the energetic position of the band-edge excitonic peak in the CER spectra (open diamonds) and values obtained from SPS measurements at room temperature (open triangles) are also displayed in Fig. 5. It should be noted that the peak positions of band-edge exciton features in the PL spectra were slightly shifted toward lower energies as compared to the corresponding transition energies obtained from CER and SPS data. The comparison between the CER (SPS) and the PL spectra allowed determining the CER-PL line shift, that was estimated to be approximately equal to 6, 8, 12, and 15 meV for $Zn_{0.95-x}Be_xMn_{0.05}Se$ crystals with Be content 0.05, 0.10, 0.15, and 0.20, respectively (see Table I). The CER spectra reflect the energetic distribution of density of states while photoluminescence data yield information on their occupation. The observed increases in the CER-PL shift with the increasing of Be content could be therefore explained by the increasing compositional disorder causing the smearing of the band-edge energies.

The full curves in Fig. 5 are least-squares fits of the temperature-dependent band-edge excitonic transition energies obtained from PL data to the Varshni semiempirical relationship as given by Eq. (2),[38]

$$E(T) = E(0) - \frac{\alpha T^2}{(\beta + T)}, \tag{2}$$

where $E(0)$ is the energy at 0 K, α and β are constants. The constant α is related to the electron (exciton)-average phonon interaction and β is closely related to the Debye temperature.[38] The values obtained for $E(0)$, α and β are listed in Table II. For comparison, the parameters $E(0)$, α and β characterizing the near-band-edge transition energy of ZB-$Zn_{0.90}Be_{0.05}Mn_{0.05}Se$,[12] ZB-$Zn_{0.75}Be_{0.05}Mn_{0.20}Se$,[12] ZB-$Zn_{0.81}Be_{0.04}Mg_{0.15}Se$,[39] ZB-ZnSe,[40] ZB-$Zn_{0.96}Be_{0.04}Se$,[41] and ZB-$Zn_{0.93}Mg_{0.07}Se$ (Ref. 41) obtained from CER measurements were also listed in Table II.

TABLE II. Values of Varshni and Bose-Einstein expression fitting parameters describing the temperature dependence of the excitonic transition energies obtained from PL data for $Zn_{0.95-x}Be_xMn_{0.05}Se$ mixed crystals. The parameters for ZB-$Zn_{0.90}Be_{0.05}Mn_{0.05}Se$, ZB-$Zn_{0.90}Be_{0.05}Mn_{0.20}Se$, ZB-$Zn_{0.81}Be_{0.04}Mg_{0.15}Se$, ZB-ZnSe, ZB-$Zn_{0.96}Be_{0.04}Se$, and ZB-$Zn_{0.93}Mg_{0.07}Se$ are included for comparison.

Samples	Feature	$E(0)$ (eV)	α (meV/K)	β (K)	a_B (meV)	Θ_B (K)
$Zn_{0.90}Be_{0.05}Mn_{0.05}Se$ [a]	X	2.879 ± 0.003	0.78 ± 0.03	250 ± 25	43 ± 4	160 ± 30
$Zn_{0.85}Be_{0.10}Mn_{0.05}Se$ [a]	X	3.004 ± 0.003	0.75 ± 0.03	250 ± 25	41 ± 4	160 ± 30
$Zn_{0.80}Be_{0.15}Mn_{0.05}Se$ [a]	X	3.156 ± 0.003	0.77 ± 0.03	250 ± 25	42 ± 4	160 ± 30
$Zn_{0.75}Be_{0.20}Mn_{0.05}Se$ [a]	X	3.346 ± 0.003	0.79 ± 0.03	250 ± 25	43 ± 4	160 ± 30
ZB-$Zn_{0.90}Be_{0.05}Mn_{0.05}Se$ [b]	E_0	2.884 ± 0.003	0.81 ± 0.03	225 ± 25	53 ± 4	175 ± 10
ZB-$Zn_{0.75}Be_{0.05}Mn_{0.20}Se$ [b]	E_0	2.897 ± 0.003	0.87 ± 0.03	225 ± 25	57 ± 4	175 ± 10
ZB-$Zn_{0.81}Be_{0.04}Mg_{0.15}Se$ [c]	E_0	3.001 ± 0.003	0.79 ± 0.03	300 ± 20	59 ± 4	210 ± 30
ZB-ZnSe[d]	E_0	2.800 ± 0.003	0.73 ± 0.04	295 ± 35	73 ± 4	260 ± 10
ZB-$Zn_{0.96}Be_{0.04}Se$ [e]	E_0	2.903 ± 0.003	0.72 ± 0.03	281 ± 20	52 ± 4	200 ± 30
ZB-$Zn_{0.93}Mg_{0.07}Se$ [e]	E_0	2.877 ± 0.003	0.73 ± 0.03	285 ± 20	54 ± 4	205 ± 30

[a]Present work (PL).
[b]Reference 12 (CER and PL).
[c]Reference 39 (PR and CER).
[d]Reference 40 (CER).
[e]Reference 41 (CER).

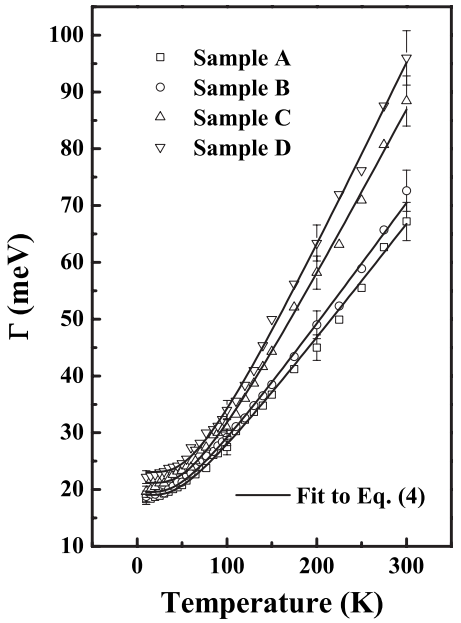

FIG. 6. Experimental data of the temperature dependence of the line width $\Gamma(T)$ of the excitonic features with representative error bars obtained from PL measurements for $Zn_{0.95-x}Be_xMn_{0.05}Se$ mixed crystals with different Be content. The full curves are least-squares fits to Eq. (4).

The temperature dependence of the band-edge excitonic transition energies could also be described by a Bose-Einstein-type expression[42]

$$E(T) = E(0) - 2a_B/[\exp(\Theta_B/T) - 1], \tag{3}$$

where $E(0)$ is the energy at 0 K, a_B represents the strength of the electron (exciton)-average phonon interaction, and Θ_B corresponds to the average phonon temperature. Shown by the dotted lines in Fig. 5 is a least-squares fit of Eq. (3) to the PL data. The obtained values for the fitting parameters are also presented in Table II. For comparison, the analogous values of fitting parameters concerning the near-band-edge transition energies obtained using contactless electroreflectance measurements for ZB-$Zn_{0.90}Be_{0.05}Mn_{0.05}Se$,[8] ZB-$Zn_{0.75}Be_{0.05}Mn_{0.20}Se$,[12] ZB-$Zn_{0.81}Be_{0.04}Mg_{0.15}Se$,[39] ZB-ZnSe,[40] ZB-$Zn_{0.96}Be_{0.04}Se$,[41] and ZB-$Zn_{0.93}Mg_{0.07}Se$ (Ref. 41) were also presented.

Taking into account the high-temperature limit of both expressions, the parameter α in Eq. (2) can be related to a_B and Θ_B in Eq. (3) that yields $\alpha = 2a_B/\Theta_B$. Comparison of the values presented in Table II shows that this relation is indeed satisfied. From Eq. (3), it is simple to show that the high-temperature limit of the slope of $E(T)$ vs T curve approaches the value of $-2a_B/\Theta_B$. The calculated values of $-2a_B/\Theta_B$ for the excitonic transitions X of $Zn_{0.95-x}Be_xMn_{0.05}Se$ mixed crystals agreed well with the value of dE_X/dT as obtained from the linear extrapolation of the high-temperature (200–300 K) PL experimental data.

The temperature dependences of the line width $\Gamma(T)$ of the band-edge exciton features obtained from PL measurements for $Zn_{0.95-x}Be_xMn_{0.05}Se$ are displayed in Fig. 6. Initially, $\Gamma(T)$ increased linearly with temperature increasing but it begins to be superlinear pattern was observed from about 150 K. The temperature dependence of the line width of excitonic emission in semiconductors could be expressed as[43]

$$\Gamma(T) = \Gamma(0) + \gamma_{AC}T + \frac{\Gamma_{LO}}{[\exp(\Theta_{LO}/T) - 1]}, \tag{4}$$

where $\Gamma(0)$ represents the broadening invoked from temperature-independent mechanisms, such as electron-electron interaction, impurity, dislocation, and alloy scattering, whereas the second term corresponds to lifetime broadening due to the exciton-acoustical phonon interaction with γ_{AC} being the acoustical phonon coupling constant. The third term is caused by the exciton-LO phonon (Fröhlich) interaction. The quantity Γ_{LO} represents the strength of the exciton-LO phonon coupling while Θ_{LO} is the LO-phonon temperature.[42,44] The full curves in Fig. 6 are least-squares fits of experimental data to Eq. (4) to evaluate $\Gamma(0)$, Γ_{LO}, Θ_{LO}, and γ_{AC} for the band-edge PL exciton feature of the investigated samples. The obtained values of $\Gamma(0)$, Γ_{LO}, Θ_{LO}, and γ_{AC} are listed in Table III. For comparison, the values of $\Gamma(0)$, Γ_{LO}, Θ_{LO}, and γ_{AC} for ZB-ZnSe (Ref. 40) and ZB-$Zn_{0.96}Be_{0.04}Se$,[41] obtained from CER measurements are also included in Table III. As shown in Table III, the value of $\Gamma(0)$ for $Zn_{0.95-x}Be_xMn_{0.05}Se$ samples is much larger than those of the previously reported Be/Mn-free sample, such as ZnSe (Ref. 40) due to mainly the poorer crystalline quality of the Be- and Mn-containing quaternary solid solutions and mentioned above chemical disorder in these crystals. The fitted value of Γ_{LO} for $Zn_{0.95-x}Be_xMn_{0.05}Se$ samples was larger than those of Be/Mn-free samples. The larger value of Γ_{LO} is presumably related to the higher effective longitudinal optical-phonon energy of the Be/Mn-containing samples. In addition, it is possible that a larger deformation-potential interaction, which may account for a significant fraction of Γ_{LO} in addition to the Fröhlich interaction, is responsible for the larger Γ_{LO} for $Zn_{0.95-x}Be_xMn_{0.05}Se$ mixed crystals.

IV. SUMMARY

In summary, the investigation of the near-band-edge transitions of high-pressure Bridgman-grown $Zn_{0.95-x}Be_xMn_{0.05}Se$ mixed crystals had been carried out by room-temperature SPS measurements, temperature-dependent PL, and CER in the range of 10–300 K. The band-edge interband transitions were observed in the SPS at room temperature. PL spectra at low temperatures consisted of an exciton line, an emission due to recombination of shallow donor-acceptor pairs, and broad bands related to the Mn^{2+} intraionic transitions. The near-band-edge transition energies determined by analyzing the CER and SPS spectra showed a blueshift with the increase in Be content. For the low-temperature CER spectra, well-resolved Rydberg's series with $n=1$ and 2 could be clearly observed for lower Be-containing $Zn_{0.95-x}Be_xMn_{0.05}Se$ solid solutions, while only a single feature was observed for the higher ($x=0.15$ and 0.20) Be-containing samples due to larger alloy disorder. As compared to the corresponding transition energies obtained from CER and SPS data, the peak positions of band-edge exciton

TABLE III. Values of the parameters that describe the temperature dependence of the broadening function $\Gamma(T)$ for edge excitonic transition of $Zn_{0.95-x}Be_xMn_{0.05}Se$ mixed-crystal samples obtained from PL spectra. The parameters for ZB-ZnSe, ZB-$Zn_{0.96}Be_{0.04}Se$, and ZB-$Zn_{0.93}Mg_{0.07}Se$ are included for comparison.

Samples	Feature	$\Gamma(0)$ (meV)	Γ_{LO} (meV)	Θ_{LO} (K)	γ_{AC} (μeV/K)
$Zn_{0.90}Be_{0.05}Mn_{0.05}Se$ [a]	X	19.1 ± 2.0	31 ± 6	200 ± 75	3 ± 1
$Zn_{0.85}Be_{0.10}Mn_{0.05}Se$ [a]	X	19.6 ± 2.0	32 ± 6	200 ± 75	3 ± 1
$Zn_{0.80}Be_{0.15}Mn_{0.05}Se$ [a]	X	21.2 ± 2.0	55 ± 6	200 ± 75	3 ± 1
$Zn_{0.75}Be_{0.20}Mn_{0.05}Se$ [a]	X	23.1 ± 2.0	64 ± 6	200 ± 75	3 ± 1
ZB-ZnSe[b]	E_0	6.5 ± 2.0	24 ± 8	360 ± 80	2[c]
ZB-$Zn_{0.96}Be_{0.04}Se$ [d]	E_0	13.7 ± 2.0	47 ± 8	250 ± 80	3 ± 1
ZB-$Zn_{0.93}Mg_{0.07}Se$ [d]	E_0	16.9 ± 2.0	50 ± 8	260 ± 80	3 ± 1

[a]Present work (PL).
[b]Reference 40 (CER).
[c]A fixed parameter.
[d]Reference 41 (CER).

features in the PL spectra were slightly shifted toward lower energies. The enlargement of the CER-PL shift value observed with the increasing of Be content could therefore be explained by the increasing compositional disorder causing the smearing of the band-edge energies. The excitonic linewidth broadening for the samples with larger Be/Zn ratio were attributed in part to the alloy-scattering effects and also to the poorer crystalline quality of the samples with higher content of Be. The fitted value of Γ_{LO} for $Zn_{0.95-x}Be_xMn_{0.05}Se$ samples was larger than those of Be/Mn-free samples. A larger deformation-potential interaction, which might account for a significant fraction of Γ_{LO} in addition to the Fröhlich interaction, is responsible for the larger Γ_{LO} for $Zn_{0.95-x}Be_xMn_{0.05}Se$ mixed crystals.

ACKNOWLEDGMENTS

The authors acknowledge the support of National Science Council of Taiwan under Project Nos. NSC 97-2811-M-011-001, NSC 97-2112-M-011-001-MY3, and NTUST-NCU International Joint Research under Project No. RP07-02.

*Present address: Institute of Applied Physics, Academy of Sciences of Moldova, 5, Academiei street, MD-2028, Chisinau, Republic of Moldova.
†Author to whom correspondence should be addressed; ysh@mail.ntust.edu.tw

[1] R. Fitzgerald, Phys. Today **53** (4), 21 (2000).
[2] S. V. Ivanov, A. A. Toropov, T. V. Shubina, A. V. Lebedev, S. V. Sorokin, A. A. Sitnikova, P. S. Kop'ev, G. Reuscher, M. Keim, F. Bensing, A. Waag, G. Landwehr, G. Pozina, J. P. Bergman, and B. Monemar, J. Cryst. Growth **214–215**, 109 (2000).
[3] S. V. Ivanov, O. V. Nekrutkina, S. V. Sorokin, V. A. Kaygorodov, T. V. Shubina, A. A. Toropov, P. S. Kop'ev, G. Reuscher, V. Wagner, J. Geurts, A. Waag, and G. Landwehr, Appl. Phys. Lett. **78**, 404 (2001).
[4] C. Vèrié, in *Semiconductors Heteroepitaxy*, edited by B. Gil and R. L. Aulombvard (World Scientific, Singapore, 1995), Vol. 1, p. 73.
[5] A. A. Wronkowska, A. Wronkowski, F. Firszt, S. Łęgowski, H. Męczyńska, A. Marasek, and W. Paszkowicz, Phys. Status Solidi C **1**, 641 (2004).
[6] M. Linnarsson, E. Janzén, B. Monemar, M. Kleverman, and A. Thilderkvist, Phys. Rev. B **55**, 6938 (1997).
[7] R. R. Gałązka, Phys. Status Solidi B **243**, 759 (2006).
[8] J. K. Furdyna, J. Appl. Phys. **64**, R29 (1988).
[9] Le Van Khoi, A. Avdonin, R. R. Gałązka, M. Lentze, C. Kehl, J. Geurts, M. Eyring, G. Astakhov, and W. Ossau, Phys. Status Solidi B **224**, 1680 (2007).
[10] E. Oh, R. G. Alonso, I. Miotkowski, and A. K. Ramdas, Phys. Rev. B **45**, 10934 (1992).
[11] M. W. Cho, J. H. Chang, D. M. Bagnall, K. W. Koh, S. Saeki, K. T. Park, Z. Zhu, K. Hiraga, and T. Yao, J. Appl. Phys. **85**, 512 (1999).
[12] H. P. Hsu, T. W. Chang, Y. S. Huang, F. Firszt, S. Łęgowski, H. Męczyńska, A. Marasek, K. Strzałkowski, K. K. Tiong, and M. Muñoz, J. Korean Phys. Soc. **53**, 77 (2008).
[13] R. Fiederling, M. Keim, G. Reuscher, W. Ossau, G. Schmidt, A. Waag, and L. W. Molenkamp, Nature (London) **402**, 787 (1999).
[14] A. A. Wronkowska, A. Bukaluk, A. Wronkowski, M. Trzciński, F. Firszt, S. Łęgowski, and H. Męczyńska, Surf. Sci. **507-510**, 170 (2002).
[15] J. Zakrzewski, F. Firszt, S. Łęgowski, H. Męczyńska, M. Pawlak, and A. Marasek, Rev. Sci. Instrum. **74**, 566 (2003).
[16] F. Firszt, K. Strzałkowski, A. J. Zakrzewski, S. Łęgowski, H. Męczyńska, and A. Marasek, Cryst. Res. Technol. **42**, 1352 (2007).
[17] F. Firszt, S. Łęgowski, H. Męczyńska, K. Szatkowski, W. Paszkowicz, and K. Godwod, J. Cryst. Growth **184–185**, 1335

(1998).
[18] W. Paszkowicz, K. Godwod, J. Domagała, F. Firszt, J. Szatkowski, H. Męczyńska, S. Łęgowski, and A. Marczak, Solid State Commun. **107**, 735 (1998).
[19] F. Firszt, A. A. Wronkowska, A. Wronkowski, S. Łęgowski, A. Marasek, H. Męczyńska, M. Pawlak, W. Paszkowicz, K. Strzałkowski, and A. J. Zakrzewski, Cryst. Res. Technol. **40**, 386 (2005).
[20] Y. S. Huang, L. Malikova, F. H. Pollak, H. Shen, P. Pamulapati, and P. Newman, Appl. Phys. Lett. **77**, 37 (2000).
[21] L. Kronik and Y. Shapira, Surf. Sci. Rep. **37**, 1 (1999).
[22] Y. S. Huang and F. H. Pollak, Phys. Status Solidi A **202**, 1193 (2005).
[23] L. Kronik and Y. Shapira, Surf. Interface Anal. **31**, 954 (2001).
[24] L. Aigouy, F. H. Pollak, J. Petruzzello, and K. Shahzad, Solid State Commun. **102**, 877 (1997).
[25] D. E. Aspnes, in *Handbook of Semiconductors*, edited by M. Balkanski (North-Holland, Amsterdam, 1980), Vol. 2, p. 109.
[26] F. H. Pollak and H. Shen, Mater. Sci. Eng. R. **10**, xv (1993).
[27] F. Rozpłoch, J. Patyk, F. Firszt, S. Łęgowski, H. Męczyńska, J. Zakrzewski, and A. Marasek, Phys. Status Solidi B **229**, 707 (2002).
[28] D. S. McClure, J. Chem. Phys. **39**, 2850 (1963).
[29] A. I. Ryskin, G. I. Khilko, B. I. Maksakov, and K. K. Dubenskii, Opt. Spectrosc. **16**, 149 (1964).
[30] C. Curie and J. S. Prener, in *Physics and Chemistry of II-VI Compounds*, edited by M. Aven and J. S. Prener (North-Holland, Amsterdam, 1967), p. 435.
[31] S. Biernacki, M. Kutrowski, G. Karczewski, T. Wojtowicz, and J. Kossut, Semicond. Sci. Technol. **11**, 48 (1996).
[32] F. Plazaola, K. Saarinen, L. Dobrzyński, H. Reniewicz, F. Firszt, J. Szatkowski, H. Męczyńska, S. Łęgowski, and S. Chabik, J. Appl. Phys. **88**, 1325 (2000).
[33] F. Plazaola, J. Flyktman, K. Saarinen, L. Dobrzyński, F. Firszt, S. Łęgowski, H. Męczyńska, W. Paszkowicz, and H. Reniewicz, J. Appl. Phys. **94**, 1647 (2003).
[34] J. A. Van Vechten and T. K. Bergstresser, Phys. Rev. B **1**, 3351 (1970).
[35] R. B. Bylsma, W. M. Becker, J. Kossut, U. Debska, and D. Yoder-Short, Phys. Rev. B **33**, 8207 (1986).
[36] S. F. Chichibu, A. Tsukazaki, M. Kawasaki, K. Tamura, Y. Segawa, T. Sota, and H. Koinuma, Appl. Phys. Lett. **80**, 2860 (2002).
[37] D. O. Dumcenco, H. P. Hsu, Y. S. Huang, F. Firszt, S. Łęgowski, H. Męczyńska, K. Strzałkowski, and K. K. Tiong, J. Appl. Phys. **103**, 093522 (2008).
[38] Y. P. Varshni, Physica (Utrecht) **34**, 149 (1967).
[39] P. J. Huang, H. P. Hsu, Y. S. Huang, F. Firszt, S. Łęgowski, H. Męczyńska, A. Marasek, and K. K. Tiong, J. Appl. Phys. **102**, 083515 (2007).
[40] L. Malikova, W. Krystek, F. H. Pollak, N. Dai, A. Cavus, and M. C. Tamargo, Phys. Rev. B **54**, 1819 (1996).
[41] H. P. Hsu, P. J. Huang, C. T. Huang, Y. S. Huang, F. Firszt, S. Łęgowski, H. Męczyńska, K. Strzałkowski, A. Marasek, and K. K. Tiong, J. Appl. Phys. **103**, 013501 (2008).
[42] S. Logothetidis, M. Cardona, P. Lautenschlager, and M. Garriga, Phys. Rev. B **34**, 2458 (1986).
[43] J. Lee, E. S. Koteles, and M. O. Vassell, Phys. Rev. B **33**, 5512 (1986).
[44] P. Lautenschlager, M. Garriga, S. Logothetidis, and M. Cardona, Phys. Rev. B **35**, 9174 (1987).